Transverse amplitude transfer experiments based on the process of spontaneous parametric downconversion

2015 Phys. Scr. 90 068013

(http://iopscience.iop.org/1402-4896/90/6/068013)

IOP Publishing | Royal Swedish Academy of Sciences Physica Scripta

Phys. Scr. **90** (2015) 068013 (13pp) doi:10.1088/0031-8949/90/6/068013

Invited Comment

Transverse amplitude transfer experiments based on the process of spontaneous parametric downconversion

Roberto Ramírez-Alarcón, Verónica Vicuña-Hernández, Héctor Cruz-Ramírez and Alfred B U'Ren

Instituto de Ciencias Nucleares,Universidad Nacional Autónoma de México, apdo. postal 70-543, 04510 DF, México

E-mail: roberto.ramirez@nucleares.unam.mx

Received 15 October 2014
Accepted for publication 4 March 2015
Published 13 May 2015

Abstract

In this work we study, for the spontaneous parametric downconversion process, how the transverse amplitude of the pump may be transferred to one of the emitted photons in a given pair when heralded by the detection of the remaining photon. We present a theoretical description of this process along with a discussion of the short-crystal regime within which faithful transfer of the transverse amplitude occurs. We show experimental results for Gaussian and Bessel–Gauss pump beams. In both cases, we verify that the transverse amplitude mechanism occurs and for the former also shows the effects of a departure from the short crystal regime. For the latter we show that our heralded single photons exhibit a non-diffractive behavior, and for orders $l = 1$ and $l = 2$ we show that these heralded single photons are in fact vortices with orbital angular momentum transferred from the pump.

Keywords: spontaneous parametric downconversion, quantum information, single photons

(Some figures may appear in colour only in the online journal)

1. Introduction

This paper is about the generation of single photons with a well-defined transverse shape, in such a way that this shape may be selected by the experimenter with relative ease [1–7]. Our approach is based on four basic ingredients. The first ingredient is the well known process of *spontaneous parametric downconversion* (henceforth referred to as SPDC) in which single photons from a laser beam, referred to as the pump, are annihilated in a non-linear crystal so as to generate photon pairs, typically referred to as signal and idler [8, 9]. The second ingredient is the use of a *structured* beam as pump in the SPDC process, with its transverse structure derived from amplitude and/or phase spatial light modulation. The third ingredient is the use of an *optical Fourier transform*, implemented through a lens, so as to resolve the two-photon state in transverse momentum space. The fourth ingredient is the use of *heralding* through which the detection of an idler photon with a well-defined transverse momentum, heralds the presence of a single photon in the signal mode. When used together, these four ingredients can yield a beautiful result: the shape—including amplitude and phase—of the pump beam, which itself may be arbitrary, may be transferred to the heralded single photons.

Why would we wish to generate single photons with a configurable transverse shape? The ability to prepare single photons with a well-defined transverse shape in fact constitutes an important enabling technology on a number of fronts. As a first example, while quantum key distribution (QKD) schemes are typically based on two-dimensional quantum systems (e.g. which employ vertical/horizontal or diagonal/anti-diagonal polarization), much can be

accomplished by extending the alphabet to more than two elements. Large-alphabet QKD schemes based on a collection of transverse modes (where the number of such modes is in principle arbitrary and thus this scheme is scalable to higher dimensions) is thus an exciting field of research [10]. As a second example, the shape of a single photon may be used to encode information, which may be stored in an atomic system when the photon is absorbed, and later retrieved, thus leading to a quantum memory [11].

Note that a single photon may be conferred a specific transverse shape in the same manner as one would proceed for a (classical) laser beam. Specifically, one would first generate photon pairs and thereafter shape one or both photons through appropriate direct spatial amplitude and/or phase modulation. In contrast, in our approach we rely on the inner workings of the SPDC process to carry out *indirect* transverse shaping of our single photons. We manipulate a Gaussian beam to be used as pump (again through amplitude and/or phase spatial modulation) to obtain the desired shape, which is then transferred to a single signal photon when heralded by the detection of an idler photon. The key advantage to this approach is that direct shaping is carried out on a high-quality Gaussian beam, rather than on the SPDC light, for which its complex spatial-spectral structure yields such direct single-photon shaping less straightforward and likewise less predictable.

The transverse amplitude transfer mechanism exploited here, does not occur for all SPDC configurations. Crystal effects, including dispersion and Poynting vector walk off, can in fact distort the transferred transverse amplitude [12, 13]. Faithful transverse amplitude transfer thus necessitates one of the following two regimes (or an appropriate combination of both): (i) a sufficiently short SPDC crystal so as to directly avoid crystal effects [1, 2, 14–20], and/or (ii) a pump beam which is sufficiently close to an idealized plane wave (or, technically, which is sufficiently compact in transverse wavevector space) so as to reduce the sensibility to these crystal effects. In this paper we analyze in some detail, both experimentally and theoretically, the so-called short crystal regime where faithful transverse amplitude transfer can occur, as well as the effects of a departure from this regime.

Within the realm of single-photon transverse spatial structure, the presence, manipulation and exploitation of orbital angular momentum (or OAM) has generated a great deal of excitement [21–27]. In the context of the SPDC process, OAM has been used as a new degree of freedom in which to demonstrate the existence of quantum entanglement [28]. In this case, entanglement resides in the OAM/optical angle pair of conjugate variables, which can behave similarly to transverse momentum/position and frequency/time pairs of variables, in which Einstein Podolsky Rosen correlations may occur [29]. A particularly promising aspect of OAM photon-pair entanglement is that it opens up a clear road towards higher-dimensional entanglement since OAM represents a discrete but infinite-dimensional photonic degree of freedom [30]. One of the key objectives in our experimental work is to show that a complex transverse spatial structure in the pump beam, in particular an optical vortex beam with OAM which includes essential phase structure, may be successfully transferred to our heralded single photons. For this purpose, we have used Bessel–Gauss beams (BG) which for orders $l \geqslant 1$ exhibit OAM.

Besides the presence of OAM, BG beams have some interesting properties which may be exploited at the single-photon level [31–33]. On the one hand, they are more resistant, as compared to an equivalent Gaussian beam, to deformation by transmission through a turbulent medium [34, 35] or due to physical obstacles [36]. On the other hand, they are non-diffractive over a certain propagation distance. In this work we have experimentally demonstrated that heralded single photons derived from a BG pump do in fact 'inherit' the non-diffractive behavior from the pump.

2. Theory

In this paper we set out to study the spatial (i.e. in transverse position/momentum) structure of photon pairs generated by the process of SPDC in a type-I, frequency-degenerate and non-collinear configuration. Our objective is to determine how the characteristics of the crystal and of the pump define the SPDC bi-photon quantum state.

The current paper is related to three previous papers from our group, [13, 37] and [38]. We utilize the SPDC process in a type-I, non-collinear, and frequency-degenerate regime, in which individual pump photons are annihilated so as to generate signal and idler photon pairs. The bi-photon SPDC quantum state can be written as $|\Psi\rangle = |\mathrm{vac}\rangle + \eta|\Psi_2\rangle$, where η is a constant related to the conversion efficiency. The two-photon component of the state, for a monochromatic pump at frequency ω_p and assuming narrowband spectral filtering of the signal and idler photons, is given by

$$|\Psi_2\rangle = \int \mathrm{d}^2\mathbf{k}_s^{\perp} \int \mathrm{d}^2\mathbf{k}_i^{\perp} S\left(\mathbf{k}_s^{\perp} + \mathbf{k}_i^{\perp}\right) \times G\left(\mathbf{k}_s^{\perp}, \mathbf{k}_i^{\perp}\right) \left|\mathbf{k}_s^{\perp}\right\rangle_s \left|\mathbf{k}_i^{\perp}\right\rangle_i, \quad (1)$$

where $|\mathbf{k}^{\perp}\rangle_{\mu} \equiv a_{\mu}^{\dagger}(\mathbf{k}^{\perp})|0\rangle$ represents a single-photon Fock state with frequency $\omega_{\mu} = \omega_p/2$ and transverse wavevector $\mathbf{k}_{\mu}^{\perp}$, with $\mu = s, i$ for the signal (s) and idler (i) photons, respectively. $S(\mathbf{k}^{\perp})$ represents the pump transverse amplitude, so that $|S(\mathbf{k}^{\perp})|^2$ is the pump angular spectrum (AS), and $G(\mathbf{k}_s^{\perp}, \mathbf{k}_i^{\perp})$ is the phase matching function given in terms of crystal properties including length, dispersion and walk off, according to

$$G\left(\mathbf{k}_s^{\perp}, \mathbf{k}_i^{\perp}\right) = \mathrm{sinc}\left[\frac{1}{2} L\, \Delta k\left(\mathbf{k}_s^{\perp}, \mathbf{k}_i^{\perp}, \right)\right] \times \exp\left(i\frac{1}{2} L \Delta k\left(\mathbf{k}_s^{\perp}, \mathbf{k}_i^{\perp}\right)\right), \quad (2)$$

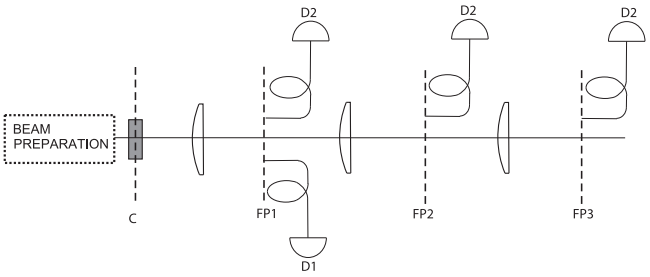

Figure 1. Experimental scheme for probing the spatial structure of SPDC photon pairs. C: crystal plane. FP1, FP2, and FP3: three different Fourier planes used in our experiments. D1 and D2: fiber tips leading to single-photon detectors.

with L the crystal length and where the phasemismatch of the process $\Delta k(\mathbf{k}_s^{\perp}, \mathbf{k}_i^{\perp})$ is given by

$$\Delta k\left(\mathbf{k}_s^{\perp}, \mathbf{k}_i^{\perp}\right) = k_p - \frac{|\mathbf{k}^{\perp}|^2}{2k_p} - k_{sz} - k_{iz} + k_y^{\perp} \tan\rho_0. \quad (3)$$

In equation (3), $k_{\mu\nu}$ (with $\mu = s, i$ and $\nu = x, y, z$) represents the Cartesian components of the k vectors for the signal and idler modes, k_p is the pump wavenumber, and $\mathbf{k}_{\mu}^{\perp}$ is a two-dimensional vector defined as $(k_{\mu x}, k_{\mu y})$. Also, we have defined $\mathbf{k}^{\perp} = \mathbf{k}_s^{\perp} + \mathbf{k}_i^{\perp}$ and ρ_0 represents the Poynting vector walkoff for the pump beam, which is assumed, without loss of generality, to occur parallel to the z–y plane.

For the exploration of the spatial structure of the photon pairs we have relied on standard Fourier optics techniques and on spatially-resolved photon counting, both in the transverse position or in the transverse wavevector domains, in single-channel and coincidence counting configurations. The general scheme used in our experiments is illustrated in figure 1.

2.1. The conditional AS

The first quantity of interest, to be referred to as the conditional angular spectrum (CAS), corresponds to the signal-mode, single-photon transverse wavevector distribution conditioned on the detection of an idler photon with transverse wavevector $\tilde{\mathbf{k}}_i^{\perp}$. The CAS can be measured through standard Fourier optics techniques, together with spatially-resolved photon counting. A lens of focal length f_1 is placed a distance of f_1 from the crystal (C plane), so that the different transverse wavevectors can be directly probed on a Fourier plane (FP1) located a distance of f_1 from the lens; see figure 1. Mathematically, this measurement is represented by the expectation value $\langle \hat{n}(\tilde{\mathbf{k}}_s^{\perp})\rangle$ taken with respect to the heralded signal-mode, single photon state $|\Psi(\tilde{\mathbf{k}}_i^{\perp})\rangle_s$, that results from the action of the projection operator

$$\hat{\Pi}\left(\tilde{\mathbf{k}}_i^{\perp}\right) = \left|\tilde{\mathbf{k}}_i^{\perp}\right\rangle_i \left\langle\tilde{\mathbf{k}}_i^{\perp}\right|_i \quad (4)$$

over the two-photon state $|\Psi_2\rangle$, obtaining

$$\left|\Psi\left(\tilde{\mathbf{k}}_i^{\perp}\right)\right\rangle_s = \int \mathrm{d}^2\mathbf{k}_s^{\perp} S\left(\mathbf{k}_s^{\perp} + \tilde{\mathbf{k}}_i^{\perp}\right) G\left(\mathbf{k}_s^{\perp}, \tilde{\mathbf{k}}_i^{\perp}\right) |\mathbf{k}_s^{\perp}\rangle_s. \quad (5)$$

Assuming detectors with ideal transverse wavevector resolution, the CAS can then be obtained as

$$R_c^{(0)}\left(\tilde{\mathbf{k}}_s^{\perp}, \tilde{\mathbf{k}}_i^{\perp}\right) = \left\langle \hat{n}\left(\tilde{\mathbf{k}}_s^{\perp}\right)\right\rangle = \left|S\left(\tilde{\mathbf{k}}_s^{\perp} + \tilde{\mathbf{k}}_i^{\perp}\right)\right|^2 \times \left|G\left(\tilde{\mathbf{k}}_s^{\perp}, \tilde{\mathbf{k}}_i^{\perp}\right)\right|^2, \quad (6)$$

where it is interesting to note that the CAS is written as the product of two separate functions. While $|S(\tilde{\mathbf{k}}_s^{\perp} + \tilde{\mathbf{k}}_i^{\perp})|^2$ depends only on the pump AS, $|G(\tilde{\mathbf{k}}_s^{\perp}, \tilde{\mathbf{k}}_i^{\perp})|^2$ depends only on crystal properties.

In a realistic experimental implementation, the transverse dimensions of the detector used are non-vanishing. For an idler angular acceptance described by the function $u_i(\mathbf{k}_i^{\perp} - \tilde{\mathbf{k}}_i^{\perp})$, centered at $\mathbf{k}_i^{\perp} = \tilde{\mathbf{k}}_i^{\perp}$, and where the contributions from each idler wavevector are summed incoherently (as is the case for our experimental conditions, see below) the two photon state (equation (1)) becomes a statistical mixture of pure states of the type given in equation (5), as follows

$$\hat{\rho}_s = \int \mathrm{d}^2\mathbf{k}_i^{\perp} u_i\left(\mathbf{k}_i^{\perp} - \tilde{\mathbf{k}}_i^{\perp}\right) \left|\Psi\left(\mathbf{k}_i^{\perp}\right)\right\rangle_s \left\langle\Psi\left(\mathbf{k}_i^{\perp}\right)\right|_s. \quad (7)$$

In this situation, the CAS of the signal-mode heralded single photon is given by

$$\mathrm{Tr}\left(\hat{n}_s\left(\mathbf{k}_s^{\perp}\right)\hat{\rho}_s\right) = \int \mathrm{d}^2\mathbf{k}_i^{\perp} u_i\left(\mathbf{k}_i^{\perp} - \tilde{\mathbf{k}}_i^{\perp}\right) R_c^{(0)}\left(\mathbf{k}_s^{\perp}, \mathbf{k}_i^{\perp}\right). \quad (8)$$

If the signal detector likewise has a non-vanishing angular acceptance described by function $u_s(\mathbf{k}_s^{\perp} - \tilde{\mathbf{k}}_s^{\perp})$, we obtain

$$R_c\left(\tilde{\mathbf{k}}_s^{\perp}, \tilde{\mathbf{k}}_i^{\perp}\right) = \int \mathrm{d}^2\mathbf{k}_s^{\perp} \int \mathrm{d}^2\mathbf{k}_i^{\perp} u_s\left(\mathbf{k}_s^{\perp} - \tilde{\mathbf{k}}_s^{\perp}\right) \times u_i\left(\mathbf{k}_i^{\perp} - \tilde{\mathbf{k}}_i^{\perp}\right) R_c^{(0)}\left(\mathbf{k}_s^{\perp}, \mathbf{k}_i^{\perp}\right). \quad (9)$$

2.2. The SPDC AS

The second quantity of interest in this study is the SPDC AS, or the rate of single-channel counts resolved on FP1; this is obtained experimentally with a detector which scans FP1 selecting single photons with transverse wavevector $\tilde{\mathbf{k}}_s^{\perp}$. Mathematically, this corresponds to $\langle \hat{n}(\tilde{\mathbf{k}}_s^{\perp})\rangle$ evaluated with respect to the two photon state in equation (1). Under the same conditions in which equation (6) was derived, it may be shown that the relationship between the AS and the CAS is as follows

$$R^{(0)}\left(\tilde{\mathbf{k}}_s^{\perp}\right) = \int \mathrm{d}^2\mathbf{k}_i^{\perp} R_c^{(0)}\left(\tilde{\mathbf{k}}_s^{\perp}, \mathbf{k}_i^{\perp}\right). \quad (10)$$

Note that when one evaluates equation (10) for (type-I, non-collinear) SPDC one obtains a well-known ring structure on the $\mathbf{k}_s^{\perp}$ plane.

If the single-photon detector used has an acceptance function $u_s(\mathbf{k}_s^{\perp} - \tilde{\mathbf{k}}_s^{\perp})$ (with a non-vanishing width), the AS is

then written as

$$R\left(\tilde{\mathbf{k}}_s^{\perp}\right) = \int \mathrm{d}^2\mathbf{k}_s^{\perp} \int \mathrm{d}^2\mathbf{k}_i^{\perp} u_s\left(\mathbf{k}_s^{\perp} - \tilde{\mathbf{k}}_s^{\perp}\right) \times R_c^{(0)}\left(\mathbf{k}_s^{\perp}, \mathbf{k}_i^{\perp}\right). \quad (11)$$

2.3. Transverse amplitude transfer and the short crystal regime

From an analysis of equation (6) it is possible to understand several important properties of the spatial structure of SPDC photon pairs. In the limit of a plane-wave pump, with transverse wavevector $\mathbf{k}_p^{\perp} = 0$, the pump AS is written as $|S(\mathbf{k}_s^{\perp} + \mathbf{k}_i^{\perp})|^2 = \delta(\mathbf{k}_s^{\perp} + \mathbf{k}_i^{\perp})$ so that if an idler photon detection event is registered with $\mathbf{k}_i^{\perp} = \tilde{\mathbf{k}}_i^{\perp}$, the signal photon will be detected a $\mathbf{k}_s^{\perp} = -\tilde{\mathbf{k}}_i^{\perp}$. The last sentence is in effect a statement of transverse momentum conservation. However, detection events are not expected at any two locations that fulfil transverse momentum conservation; only at those that in addition lead to a non-vanishing $|G(-\tilde{\mathbf{k}}_i^{\perp}, \tilde{\mathbf{k}}_i^{\perp})|^2$ function. Extending this situation, we can consider a pump which departs from a delta function, i.e. which is described as a superposition of plane waves. In this situation, a single-photon detection event with $\mathbf{k}_i^{\perp} = \tilde{\mathbf{k}}_i^{\perp}$, will be correlated to a detection event within a region *around* $\mathbf{k}_s^{\perp} = -\tilde{\mathbf{k}}_i^{\perp}$ with an uncertainty determined by the CAS, which itself has a width which depends on the pump AS width.

A typical experimental situation may be modelled by a pump in the form of a Gaussian beam, with beam waist parameters W_x and W_y along the x and y directions leading to the following pump AS

$$\left|S\left(\mathbf{k}_s^{\perp} + \mathbf{k}_i^{\perp}\right)\right|^2 = \exp\left(-\frac{1}{2}\left\{W_x^2\left(k_{sx}^{\perp} + k_{ix}^{\perp}\right)^2 + W_y^2\left(k_{sy}^{\perp} + k_{iy}^{\perp}\right)^2\right\}\right), \quad (12)$$

where $k_{\mu\nu}^{\perp}$ (with $\mu = s, i$ and $\nu = x, y$) are the x and y components of the transverese wavevectors $\mathbf{k}_s^{\perp}$ and $\mathbf{k}_i^{\perp}$. Increasing the degree of focusing, or alternatively reducing the values of W_x and W_y, leads to an increased width of the AS and CAS functions, the latter as limited by the width of the function $|G(\mathbf{k}_s^{\perp}, \mathbf{k}_i^{\perp})|^2$. Thus, while in the limit of a plane-wave pump, a signal photon with transverse wavevector $\mathbf{k}_s^{\perp}$ corresponds to an idler photon with a well defined wavevector–$\mathbf{k}_s^{\perp}$, this is no longer the case as the degree of focusing is increased.

Another important property of the spatial structure of photon pairs can be immediately derived from equation (6). If the function $|G(\tilde{\mathbf{k}}_s^{\perp}, \tilde{\mathbf{k}}_i^{\perp})|^2$ is broader than the function $|S(\tilde{\mathbf{k}}_s^{\perp} + \tilde{\mathbf{k}}_i^{\perp})|^2$, the former can be considered constant in the region of interest. The CAS is then identical to the pump AS except displaced by—$\tilde{\mathbf{k}}_i^{\perp}$ in transverse wavevector space. Applying the same argument at an amplitude rather than intensity level, see equation (5), it becomes apparent that this mechanism is in fact phase-preserving so that it is the full transverse amplitude of the pump which may be transferred to the signal-mode, single-photon transverse amplitude. Note that while it is possible to shape single photons through appropriate *post-production* projection. i.e. using amplitude and/or phase filters, in our approach signal-mode single photons are generated already with the desired shape inherited from the pump, which can be revealed through the heralding process.

In what follows, we investigate in greater detail the conditions under which the transverse amplitude is transferred faithfully from the pump to the heralded single photons. Following the detailed analysis presented in [13], the function $|G(\tilde{\mathbf{k}}_s^{\perp}, \tilde{\mathbf{k}}_i^{\perp})|^2$ is determined by the SPDC crystal, in such a way that its width in transverse wavevector space δk_G depends inversely on the crystal length L. Likewise, the function $|S(\tilde{\mathbf{k}}_s^{\perp} + \tilde{\mathbf{k}}_i^{\perp})|^2$ is determined solely by the pump, in such a way that its width δk_S corresponds directly to the pump width in transverse wavevector space. If $L_c(\delta k_S)$ denotes the crystal length such that $\delta k_S = \delta k_G$ it then follows that the amplitude transfer mechanism is valid for $L \ll L_c(\delta k_S)$ (i.e. for $\delta k_S \ll \delta k_G$); we refer to this regime as the short-crystal regime [12, 20, 39–43].

Figure 2(a) shows, as a specific example, in the background: a simulation of the SPDC AS (equation (11)) for a β barium borate (BBO) crystal of 1 mm length and a Gaussian pump beam centered at 406.8 nm with $W_x = W_y = 30\ \mu$m (corresponding to $\delta k_S/2 = \delta k = 0.047\ \mu\mathrm{m}^{-1}$), and in the foreground: simulations of the CAS (equation (9)) corresponding to seven values of ϕ_i (shown as white disks) appearing at equal angular intervals on the $k_{sx} < 0$ side of the AS. For three specific points ($\phi_i = 90°, 180°, 270°$) we show in addition plots of the $|S(\tilde{\mathbf{k}}_s^{\perp} + \tilde{\mathbf{k}}_i^{\perp})|^2$ and $|G(\tilde{\mathbf{k}}_s^{\perp}, \tilde{\mathbf{k}}_i^{\perp})|^2$ functions, from which one obtains the CAS when multiplied together. Note that while δk_S remains unchanged around the SPDC annulus, both δk_G and the orientation of $|G(\tilde{\mathbf{k}}_s^{\perp}, \tilde{\mathbf{k}}_i^{\perp})|^2$ vary as a function of ϕ_i. This implies that L_c depends both on δk_S and on ϕ_i, as indicated in figure 2(b). Note that, interestingly, the short-crystal regime (region under the curves in figure 2(b)), within which the transverse amplitude may be faithfully transferred, can be significantly expanded for $\phi_i = 270°$ as compared to $\phi_i = 90°$ and $\phi_i = 180°$.

In the short-crystal regime, the signal-mode heralded single photon is determined solely by the pump, i.e. the crystal properties play no role. In particular, the transverse amplitude becomes a displaced version of the pump transverse amplitude, i.e.

$$\left|\Psi\left(\tilde{\mathbf{k}}_i^{\perp}\right)\right\rangle_s = \int \mathrm{d}\mathbf{k}_s^{\perp} S\left(\mathbf{k}_s^{\perp} + \tilde{\mathbf{k}}_i^{\perp}\right) \left|\mathbf{k}_s^{\perp}, \omega_p - \tilde{\omega}_i\right\rangle_s, \quad (13)$$

while the CAS is identical to the pump AS, except displaced, i.e.

$$R_c^{(0)}\left(\tilde{\mathbf{k}}_s^{\perp}, \tilde{\mathbf{k}}_i^{\perp}\right) = \left|S\left(\tilde{\mathbf{k}}_s^{\perp} + \tilde{\mathbf{k}}_i^{\perp}\right)\right|^2. \quad (14)$$

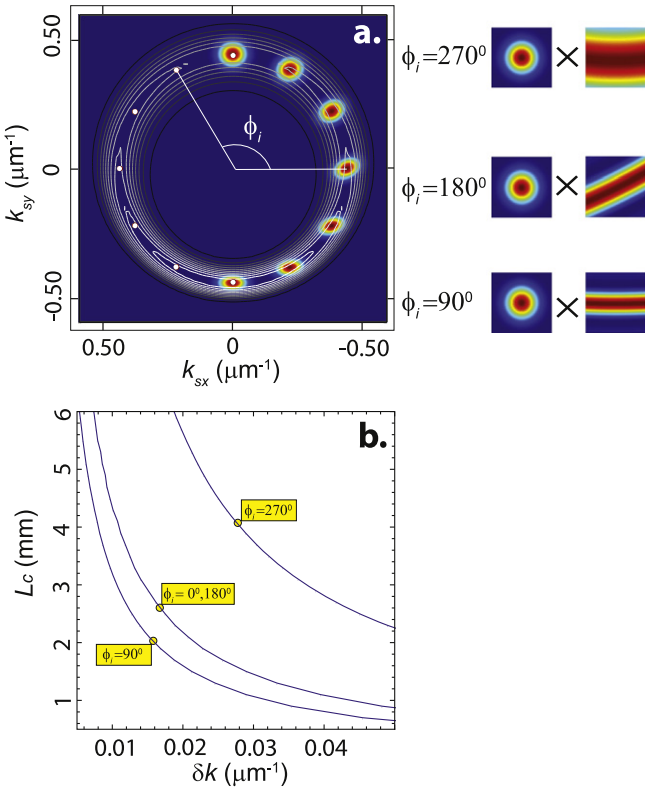

Figure 2. (a) Background: contour plot of the SPDC AS. Foreground: white disks indicate locations of the fixed conditioning detector, on the $k_{sx} < 0$ half of the SPDC angular spectrum, separated at equal angular intervals of 30°. To each of these disks corresponds a CAS function shown on the diametrically opposed portion of the angular spectrum. For three specific disks, we present in addition plots of $|S(\tilde{\mathbf{k}}_s^{\perp} + \tilde{\mathbf{k}}_i^{\perp})|^2$ (equation (12)) and $|G(\tilde{\mathbf{k}}_s^{\perp}, \tilde{\mathbf{k}}_i^{\perp})|^2$ (equation (2)), from which one obtains the CAS when multiplied together. (b) Critical length L_c plotted as a function of the pump beam width δk in transverse k-vector space, for a fixed idler detector location ϕ_i.

2.4. The conditional transverse intensity (CTI) and the SPDC transverse intensity (TI)

So far, we have studied SPDC light in the transverse wavevector domain. We are also interested in the picture provided by the transverse position domain. This leads to a third quantity of interest, namely the CTI of the signal-mode, heralded single photon, which is evaluated in the transverse position $\boldsymbol{\rho}_s^{\perp}$ rather than the transverse wavevector $\mathbf{k}_s^{\perp}$.

This quantity can be measured through spatially-resolved photon counting on a Fourier plane (FP2) located at distance $2f_2$ from FP1, with a lens of focal length f_2 placed symmetrically between FP1 and FP2. Mathematically, this measurement is represented by the expectation value $\mathrm{Tr}\,(\hat{n}_s(\tilde{\boldsymbol{\rho}}_s^{\perp})\hat{\rho}_s)$, defined in terms of annihilation operators in the transverse position domain $\hat{a}_\mu(\boldsymbol{\rho}^{\perp}) = (4\pi^2)^{-1}\int \mathrm{d}\mathbf{k}^{\perp} \mathrm{e}^{\mathrm{i}\mathbf{k}^{\perp}\cdot\boldsymbol{\rho}^{\perp}}\hat{a}_\mu(\mathbf{k}^{\perp})$, and evaluated with respect to a mixed state in the form of equation (7), with the reduced signal-mode heralded single photon state (equation (13)), as

$$\mathscr{R}_c\left(\tilde{\boldsymbol{\rho}}_s^{\perp}\right) = \int \mathrm{d}\mathbf{k}_i^{\perp} u\left(\mathbf{k}_i^{\perp} - \tilde{\mathbf{k}}_i^{\perp}\right) \times \left|\frac{1}{(2\pi)^2}\int \mathrm{d}\mathbf{k}_s^{\perp} \mathrm{e}^{\mathrm{i}\mathbf{k}_s^{\perp}\cdot\tilde{\boldsymbol{\rho}}_s^{\perp}} S\left(\mathbf{k}_s^{\perp} + \mathbf{k}_i^{\perp}\right)\right|^2. \quad (15)$$

Applying the shift theorem, and noting that the phase $\exp(i\rho_s^{\perp}\cdot\tilde{\mathbf{k}}_i^{\perp})$ is suppressed by the absolute value, the integral over $\tilde{\mathbf{k}}_i^{\perp}$ becomes simply a constant M_2 and the heralded single photon CTI reduces to

$$\mathscr{R}_c\left(\tilde{\boldsymbol{\rho}}_s^{\perp}\right) = M_2\left|\mathscr{S}\left(\tilde{\boldsymbol{\rho}}_s^{\perp}\right)\right|^2, \quad (16)$$

in terms of the Fourier transform of the pump transverse amplitude $\mathscr{S}(\tilde{\boldsymbol{\rho}}_s^{\perp})$. In the derivation of equation (16) we have considered an idler-mode conditioning detector with a non-vanishing transverse acceptance. Then, interestingly, the signal-mode heralded single photon CTI is identical in shape to the pump TI, despite averaging over the angular acceptance of the idler detector.

The fourth quantity of interest is the SPDC TI, which corresponds to the spatially resolved rate of single-channel counts on FP2. Mathematically this corresponds to $\langle\hat{n}_s(\tilde{\boldsymbol{\rho}}_s^{\perp})\rangle$, where the expectation value is computed with respect to the two-photon state (see equation (1)). This leads to the following expression

$$\mathscr{R}\left(\tilde{\boldsymbol{\rho}}_s^{\perp}\right) = \int \mathrm{d}\mathbf{k}_i^{\perp} \times \left|\frac{1}{(2\pi)^2}\int \mathrm{d}\mathbf{k}_s^{\perp} \mathrm{e}^{\mathrm{i}\mathbf{k}_s^{\perp}\cdot\tilde{\boldsymbol{\rho}}_s^{\perp}} S\left(\mathbf{k}_s^{\perp} + \mathbf{k}_i^{\perp}\right)\right|^2, \quad (17)$$

which is similar to that in equation (15), except that the integration domain for $\mathbf{k}_i^{\perp}$ is unconstrained. Again applying the shift theorem, this can be reduced to

$$\mathscr{R}\left(\tilde{\boldsymbol{\rho}}_s^{\perp}\right) = M_1\left|\mathscr{S}\left(\tilde{\boldsymbol{\rho}}_s^{\perp}\right)\right|^2, \quad (18)$$

where M_1 is a constant proportional to the the idler-mode flux. Because the domain of integration for M_1 is unconstrained as opposed to that for M_2, clearly $M_1 > M_2$. Apart from the difference in count rate, the heralded single photon CTI (equation (16)) and the SPDC TI (equation (18)), interestingly have identical shapes.

The fact that the functions $\mathscr{R}_c(\tilde{\boldsymbol{\rho}}_s^{\perp})$ and $\mathscr{R}(\tilde{\boldsymbol{\rho}}_s^{\perp})$ are identical implies that there are no signal-idler spatial correlations between the idler-mode conditioning photons collected on FP1 and the signal-mode conditioned photons detected on FP2. In other words, a small shift in the position of the conditioning detector on FP1 will not lead to a modified spatial structure of the conditioned photon resolved on FP2. This can be understood also, with the help of the Fedorov criterion for the presence of correlations [44], which

essentially equates the ratio of the width of the single-channel count distribution to the width of the coincidence count distribution with the strength of the correlations.

It is surprising that while the two-photon state is entangled in transverse wavevector, propagation of the signal and idler photons through specific optical systems can render the transverse *position* correlations essentially non-existent. The joint amplitude which characterizes the two-photon state evidently has both amplitude and phase; while the overall entanglement in both amplitude and phase must remain constant as the signal and idler propagate through arbitrary lossless optical systems, the measured joint spatial *intensity* suppresses phase information. Thus, it becomes possible for entanglement to fully migrate to the phase so that when measuring the joint intensity on specific planes of detection (in our case FP1 for the idler and FP2 for the signal), the correlations essentially vanish [45, 46].

The discussion in the previous paragraph is linked to the treatment of SPDC propagation through fractional Fourier transforms, see [47]; in that work, the independent transit of the signal and idler photons through post-generation optical systems is characterized by phases α (for the signal) and β (for the idler). It is shown that for $\alpha + \beta = 0 \pmod{2\pi}$ transverse position correlations are maximal and positive, for $\alpha + \beta = \pi \pmod{2\pi}$ transverse position correlations are maximal and negative, and for $\alpha + \beta = 3\pi/2 \pmod{2\pi}$ transverse position correlations are minimized. Each Fourier transform (e.g. from the C to the FP1 planes, and from the FP1 to the FP2 planes) leads to a phase of $\pi/2$. While the idler detected on FP1 leads to $\beta = \pi/2$, the signal collected on FP2 leads to $\alpha = \pi$ so that $\alpha + \beta = 3\pi/2$.

2.5. BG pump beams: non-diffractive behavior and OAM

The discussion presented so far is applicable for an arbitrary pump beam. We have seen that for a sufficiently thin crystal and/or a sufficiently compact pump beam in transverse wavevector space (short-crystal regime), the transverse amplitude of the pump may be transferred to a signal-mode heralded single photon when conditioned by the detection of an idler photon with a well-defined transverse wavevector.

In actual experiments, we are therefore free to use a pump beam according to particular needs. In our own experimental work (see next section), we initially used a Gaussian pump beam, for which we on the one hand verified that faithful transverse amplitude transfer indeed occurs within the short-crystal regime, and on the other hand we observed the effects of departing from this short-crystal regime.

We also used a second class of pump beams, namely BG beams, which exhibit a number of interesting properties. A BG beam is a conical coherent superposition of Gaussian beams, each with a radius at the beamwaist parameter w_0, and with a cone opening half-angle $\arcsin(k_t/k_p)$, where k_t is the transverse wavenumber and k_p is the pump wavenumber. For a BG beam of order l, the transverse amplitude can be written as

$$S\left(\mathbf{k}^{\perp}\right) = A \exp\left(-\frac{w_0^2}{4}|\mathbf{k}^{\perp}|^2\right) \times I_l\left(\frac{k_t w_0^2 |\mathbf{k}^{\perp}|}{2}\right) \exp(il\phi), \tag{19}$$

where A is a normalization constant, $I_l(.)$ is an lth order modified Bessel function of the first kind and $\phi = \arctan(k_y/k_x)$ [33]. The w_0 parameter may be obtained from the width $\Delta\kappa$ of the characteristic annular shape of the BG beam AS $|S(\mathbf{k}^{\perp})|^2$, according to the relationship $w_0 = 4/\Delta\kappa$. When viewed in the transverse position $\boldsymbol{\rho}^{\perp}$ domain, the transverse amplitude as a function of the propagation distance z becomes

$$A_p\left(\boldsymbol{\rho}^{\perp}\right) = A' \frac{1}{\mu} \exp\left\{-\frac{1}{\mu}\left(\frac{ik_t^2 z}{2k_p} + \frac{|\boldsymbol{\rho}^{\perp}|^2}{w_0^2}\right)\right\} \times J_l\left(\frac{k_t|\boldsymbol{\rho}^{\perp}|}{\mu}\right), \tag{20}$$

in terms of $\mu = 1 + iz/z_r$ with $z_r = k_p w_0^2/2$ the Rayleigh range of the pump, the lth-order Bessel function $J_l(.)$ and a normalization constant A′.

There are two noteworthy properties of BG beams which relate to our initial motivation to use these beams. On the one hand, BG beams of all orders exhibit a non-diffractive behavior. Indeed, the beam has a TI which remains essentially unchanged over a propagation distance $z_{max} = 2w_0 k_p/k_t$, where k_p is the pump wavenumber. On the other hand, for orders $l \geqslant 1$, BG beams exhibit OAM with a topological charge l. Within the short crystal regime, in which the transverse amplitude of the pump beam is faithfully transferred to the heralded single photons, we expect that both of these properties, non-diffractive behavior and the presence of OAM, will likewise be transferred to the heralded single photon. Note that because an optical vortex is fundamentally defined by a phase $\exp(il\phi)$, a vortex pump in the SPDC process is ideal to demonstrate transverse amplitude transfer to a heralded daughter photon.

The ability to control the transverse spatial intensity pattern at the single photon level, while also achieving non-diffracting behavior, is notable. Applications could be found in the area of free-space quantum communications, where the ability of a non diffracting beam to maintain its form despite the presence of obstacles [48] and/or despite propagation through a turbulent medium [49, 50] would be particularly useful. Applications could likewise be found in the controlled interaction of single photons with atoms and/or ions in the linear arrangement of an ion trap or an optical lattice.

3. Experimental results

The general scheme used in our experiments is summarized in figure 1. In all cases, a BBO crystal of 1 mm length, placed on

plane C, was used for the generation of SPDC photon pairs. A diode laser centered at 406.8 nm with ~100 mW power was used as pump.

3.1. Gaussian beam pump

Our first experiment involved a Gaussian beam pump; details of this experiment are presented in [13]. The beam from the diode laser was spatially filtered so as to obtain a high-quality Gaussian beam with measured waist parameters $W_x = 182.0\ \mu$m and $W_y = 189.0\ \mu$m (see equation (12)); when used directly, this pump beam will be referred to as configuration 1. Our approach was to vary the degree of focusing, characterized by parameters W_x and W_y, so as to control whether or not the source is in the short-crystal regime (the beamwaist W_0, taken here as the average of W_x and W_y, corresponds to a region in transverse wavevector space of radius $\delta k = \sqrt{2}/W_0$). Thus, for configuration 1 we have $\delta k = 0.0076\ \mu\text{m}^{-1}$. Focusing the beam using a $f = 6$ cm focal length lens, we obtained a Gaussian beam with measured waist parameters $W_x = 38.9\ \mu$m and $W_y = 34.7\ \mu$m, to be referred to as configuration 2 (corresponding to $\delta k = 0.038\ \mu\text{m}^{-1}$).

The SPDC photons are transmitted through a $\lambda > 490$ nm long wave pass filter followed by a bandpass filter centered at 810 nm with a 10 nm bandwidth, so as to suppress pump photons and restrict the SPDC bandwidth. An *f–f* optical system is used in order to yield a Fourier plane (FP1 in figure 1) on which we can probe the signal and idler transverse momentum distributions. Specifically, a $f_1 = 10$ cm focal length lens is placed at a distance of 10 cm from the C plane, which defines FP1 at a distance of 10 cm from the lens.

The CAS is measured using spatially-resolved conditional photon counting on FP1. For this purpose, we have used *two* independent fiber tips of large-diameter fiber (200 μm core diameter), placed at diametrically-opposed regions of the SPDC annulus; while one fiber tip (corresponding to the idler photon) is left in a fixed position, the other fiber tip (corresponding to the signal photon) can be displaced laterally along the x and y directions with the help of a computer-controlled motor (50 nm resolution and 1.5 cm travel range). The fibers lead to Si avalanche photodiodes (D1 and D2), with their outputs connected to standard pulse-counting equipment to obtain number of detection events per second data.

In order to study the behavior of the transverse amplitude transfer mechanism for configurations 1 and 2 (see above), we compare the measured CAS, with the AS of the pump beam (plotted from equation (12)) and the numerically obtained CAS (from a simulation based on equation (9)). In the experiment, we placed the conditioning detector at point with $\phi_i = 180°$ (see figure 2(a), involving $k_{iy}^{\perp} = 0$ and a $k_{ix}^{\perp}$ value which maximizes the counts). The signal-mode detector (D2) is then scanned around the diametrically-opposed point, in an area centered around the point for which transverse momentum conservation is fulfilled. Note that the fiber used for idler-mode collection is highly multi-mode and its angular acceptance function corresponds to the function $u(\mathbf{k}_i^{\perp} - \tilde{\mathbf{k}}_i^{\perp})$, which we model as a Gaussian function with a full width at $1/e$ of 200 μm. Detection over many transverse fiber modes leads to the incoherent sum over idler transverse wavevectors in equation (7).

In figure 3, the top/bottom row corresponds to configuration 1/2. In figures 3(a) and (d) we show the experimentally measured CAS, while in 3(b) and (e) we show corresponding numerical simulations obtained from equation (9); note the excellent agreement between measurements and simulations. Figures 3(c) and (f) show the AS of the Gaussian pump beam used in the experiment, plotted from equation (19). For the measurements shown in panels 3(a) and (d), data was taken on a grid of transverse position values, centered around a transverse position diametrically opposed to the location of the idler-mode fiber. Grid points are characterized by the fiber tip's transverse position $\boldsymbol{\rho}_{s0}^{\perp}$, corresponding to transverse momentum $\mathbf{k}_{s0}^{\perp} = [\omega_s/(cf_1)]\boldsymbol{\rho}_{s0}^{\perp}$. The transverse dimensions of the fiber core which collects photons are indicated by a white circle which is shown in each panel's bottom-left corner. In some cases, the transverse width of the collection fiber can be significant when compared to the CAS width.

It is evident from figure 3 that for configuration 1, the CAS closely resembles the pump AS in shape, as is expected since this configuration lies within the short-crystal regime. In contrast, for configuration 2 the CAS is elongated and tilted and does not resemble the pump AS; again, this is expected since this configuration is not in the short-crystal regime.

3.2. Bessel gauss pump

The use of a Gaussian beam pump discussed in the previous subsection served to verify our correct understanding of AS transfer through heralding in the SPDC process. However, we also carried out experiments with a pump exhibiting greater spatial structure, in particular BG beams, which exhibit non-diffractive behavior and, for $l \geqslant 1$ orders, contain OAM; details of these experiments are presented in [37] and [38].

In our experiments, we have prepared a BG beam with a topological charge of $l = 0$, $l = 1$ or $l = 2$, to be used as pump in the SPDC process. The beam from a diode laser is first magnified appropriately, using a first telescope, so as to illuminate an axicon, i.e. a conical lens, which maps the incoming Gaussian beam to a BG beam of order 0. The k_t parameter of the BG beam (see equation (19)) can then be controlled with a second telescope placed following the axicon. For orders 1 and 2, a vortex phase plate (a device which imparts a linear azimuthal phase gradient covering 0 to 2π radians for order 1 or 0 to 4π radians for order 2) is placed on the internal Fourier plane in the second telescope.

Figure 4 shows for the prepared BG beams, measurements of the TI (in the first column) and the AS (in the second column), obtained with a high-resolution CCD camera; orders 0, 1 and 2 are shown on the first, second, and third row respectively. While the TI was measured by a CCD camera on the C plane, the AS was measured using an *f–f* system with its

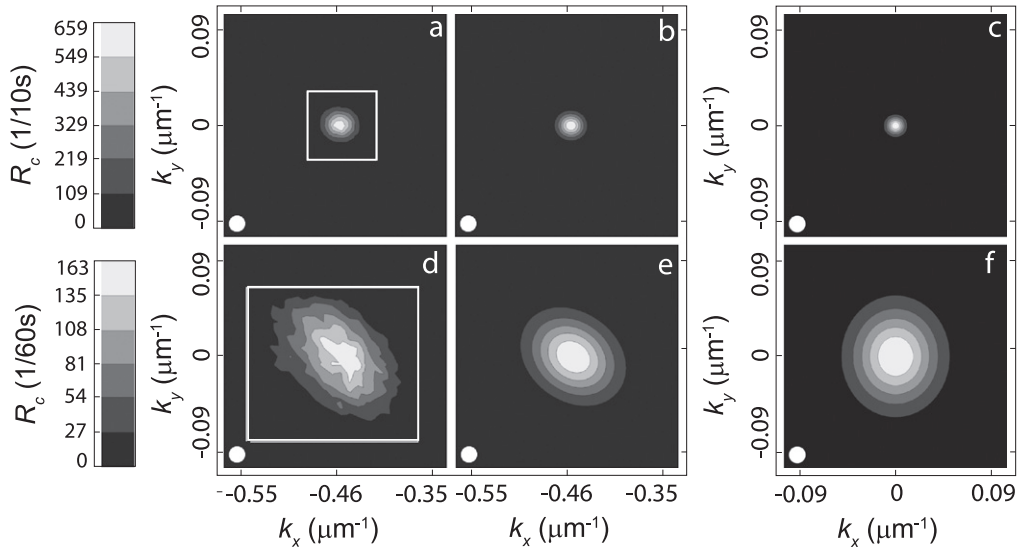

Figure 3. Measured (a), (d) and numerically calculated (b), (e) CAS (through equation (9)) of the signal-mode heralded single photon. AS of the Gaussian pump beam (c), (f), plotted from equation (19). First row: configuration 1, second row: configuration 2.

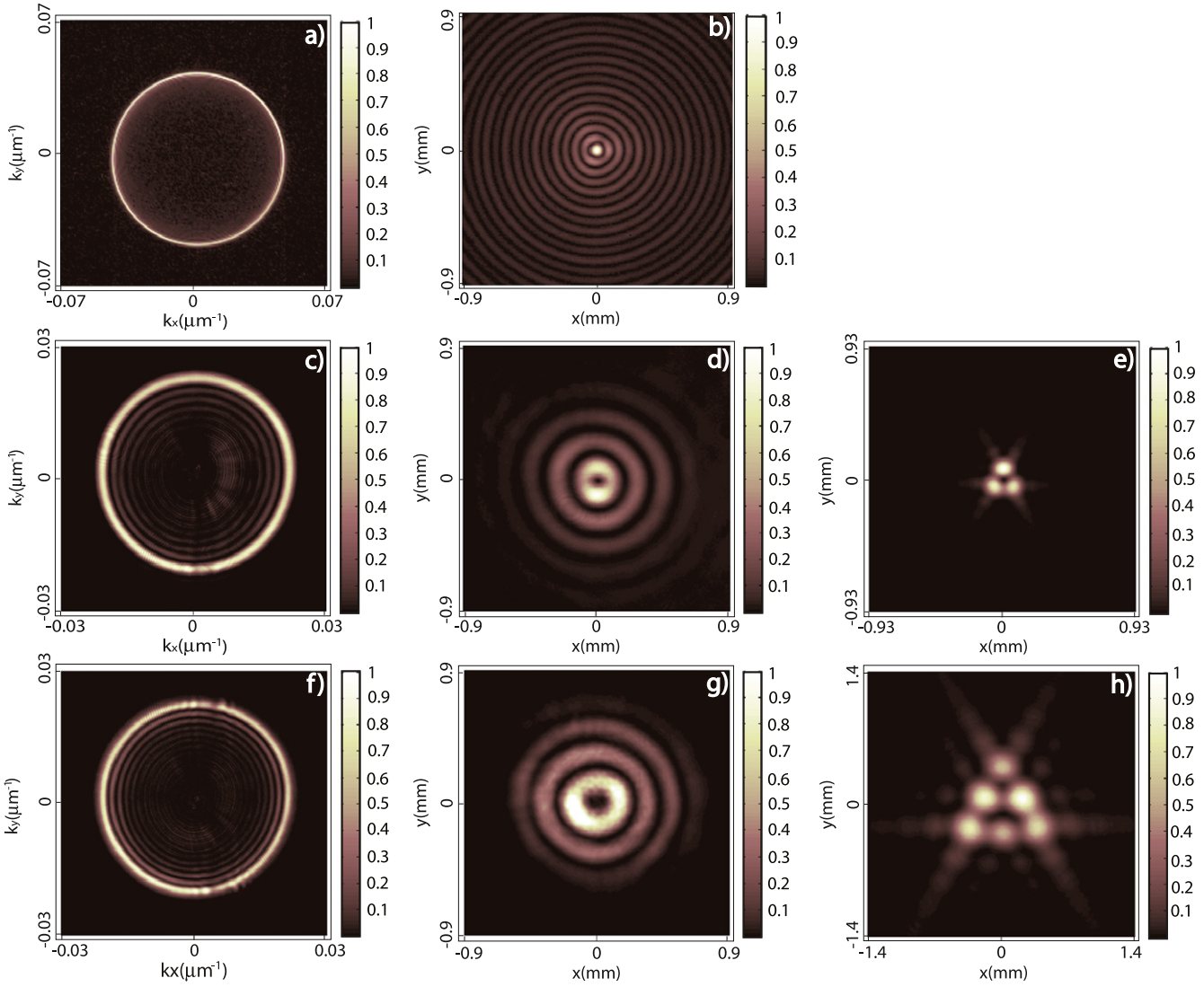

Figure 4. BG pump properties: (a), (c), (f) Measured angular spectrum, (b), (d), (g) measured transverse intensity, (e), (h) far-field diffraction pattern through an triangular aperture. First row: $l = 0$, second row: $l = 1$,and third row: $l = 2$.

input plane coinciding with the C plane and a CCD camera on its output plane.

In figure 4(b), for an $l = 0$ order BG beam, we may appreciate the expected transverse shape, i.e a central spot surrounded by a set of concentric rings, and the corresponding AS in figure 4(a), i.e. an annulus with radius k_t and width $\Delta k = 4/w_0$. The measured values of k_t are $0.046\,\mu\text{m}^{-1}$, $0.022\,\mu\text{m}^{-1}$, and $0.022\,\mu\text{m}^{-1}$ for $l = 0$, $l = 1$, and $l = 2$ respectively. Likewise, in the second and third rows, for $l = 1$ and $l = 2$ leading to the presence of OAM, we may appreciate the expected shape, i.e. a central intensity null (which is consistent with a phase singularity) surrounded by concentric rings and the corresponding AS which is similar to the $l = 0$ AS. The slight departure from azimuthal symmetry can be attributed to imperfections of the axicon and/or vortex phase plate.

In our experimental work we exploit a technique pioneered by Hickmann *et al* [51–53], through which the topological charge of an optical vortex beam can be revealed via the far-field diffraction pattern through a triangular aperture. Specifically, it was found in the cited papers that the far-field diffraction pattern of an optical vortex with the phase singularity aligned with the center of a triangular aperture is formed by a triangular arrangement of intensity lobes, with the number of such lobes correlated to the topological charge. The topological charge m is then given by $N - 1$ where N is the number of lobes (discounting secondary lobes) on any side of the triangular intensity pattern. In our experimental work, we use this technique in order to characterize the OAM properties of, both, pump and SPDC light.

The third column in figure 4 shows, for orders $l = 1$ and $= 2$, the far field diffraction pattern through a triangular aperture. The expected intensity distributions involving three lobes for $l = 1$ (figure 4(e)) and six lobes for $l = 2$ (figure 4(h)) can be readily appreciated, thus verifying the presence of OAM in the pump beam.

In order to visualize the propagation properties of the BG pump beams, figure 5 shows a plot of the measured transverse pump intensity distribution along the y direction, measured with a CCD camera, as a function of the propagation distance z (with $z = 0$ on the C plane). Panels a, b , and c correspond to BG beams of order 0, 1, and 2, respectively. Note that in all three cases there is a significant propagation distance over which the TI remains essentially unchanged. We found that for the $l = 1$ and $l = 2$ beams, the non-diffractive distance is somewhat less than for the $l = 0$ beam, probably because of imperfections in the vortex phase plates.

Figure 6 shows the spatial properties of the photon pairs as measured on FP1. While the first, second and third row corresponds to topological charge 0, 1, and 2, respectively, the first column corresponds to the measured AS, and the second column corresponds to the measured CAS. The AS measurement is obtained by scanning a fiber tip on FP1, leading to a single-photon detector; this represents the well-known SPDC annulus which for a Bessel–Gauss pump can have an asymmetry related to pump Poynting vector walk off, which is most evident in panel (a). The CAS measurement is carried out by placing a fiber tip leading to a conditioning

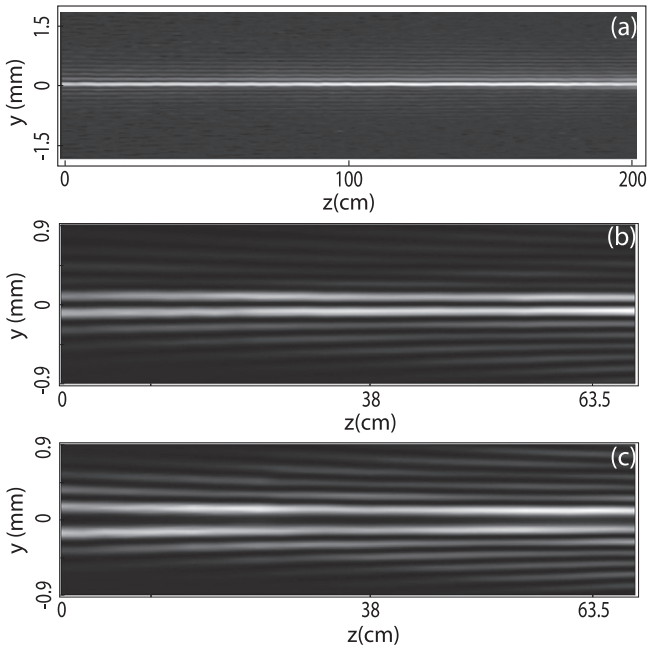

Figure 5. Non-diffracting behavior in propagation of the BG pump beam of order: (a) $l = 0$, (b) $l = 1$ and (c) $l = 2$.

detector at the location indicated by a dot on the right hand side of the AS (panels a, d and g) and scanning a second tip, leading to a second detector, around the diametrically opposed point. For these three configurations, the idler collection is centred at $\phi_i = 270°$ ensuring for our experimental parameters, that these configurations are in the short-crystal regime. Therefore, the CAS should be ideally identical in shape to the pump AS. The fact that the former has a greater width is related to the transverse width of the conditioning and scanning fiber tips.

By placing a second lens (L2, focal length $f = 15$ cm) at a distance of 15 cm from FP1, we can define a second Fourier plane (FP2) a distance of 15 cm from the lens (see figure 1). In figure 7 we show measurements of the SPDC TI, obtained by a single scanning fiber tip (with 50 μm diameter) on FP2 leading to pulse-counting equipment. In this figure we also show measurements of the CTI, for which the conditioning fiber tip (with 200 μm diameter) is still on FP1 while the scanning fiber tip (with 50 μm diameter) is on FP2. While the first, second and third row corresponds to topological charge 0, 1, and 2, respectively, the first column corresponds to the measured TI, and the second column corresponds to the measured CTI. Note the TI and CTI are essentially identical in shape, as expected from equations (16) and (18).

Because BG beams are non-diffractive, and our BG-pump experimental configurations are in the short-crystal regime, we expect that the signal-mode heralded single photons will likewise be non-diffractive. In order to study the propagation properties of the heralded single photons we have displaced the plane on which the signal-mode fiber tip is scanned, from its initial position corresponding to the plane FP2 (regarded as $z = 0$), and have collected signal-idler coincidence data for each propagation plane. In figure 8 we

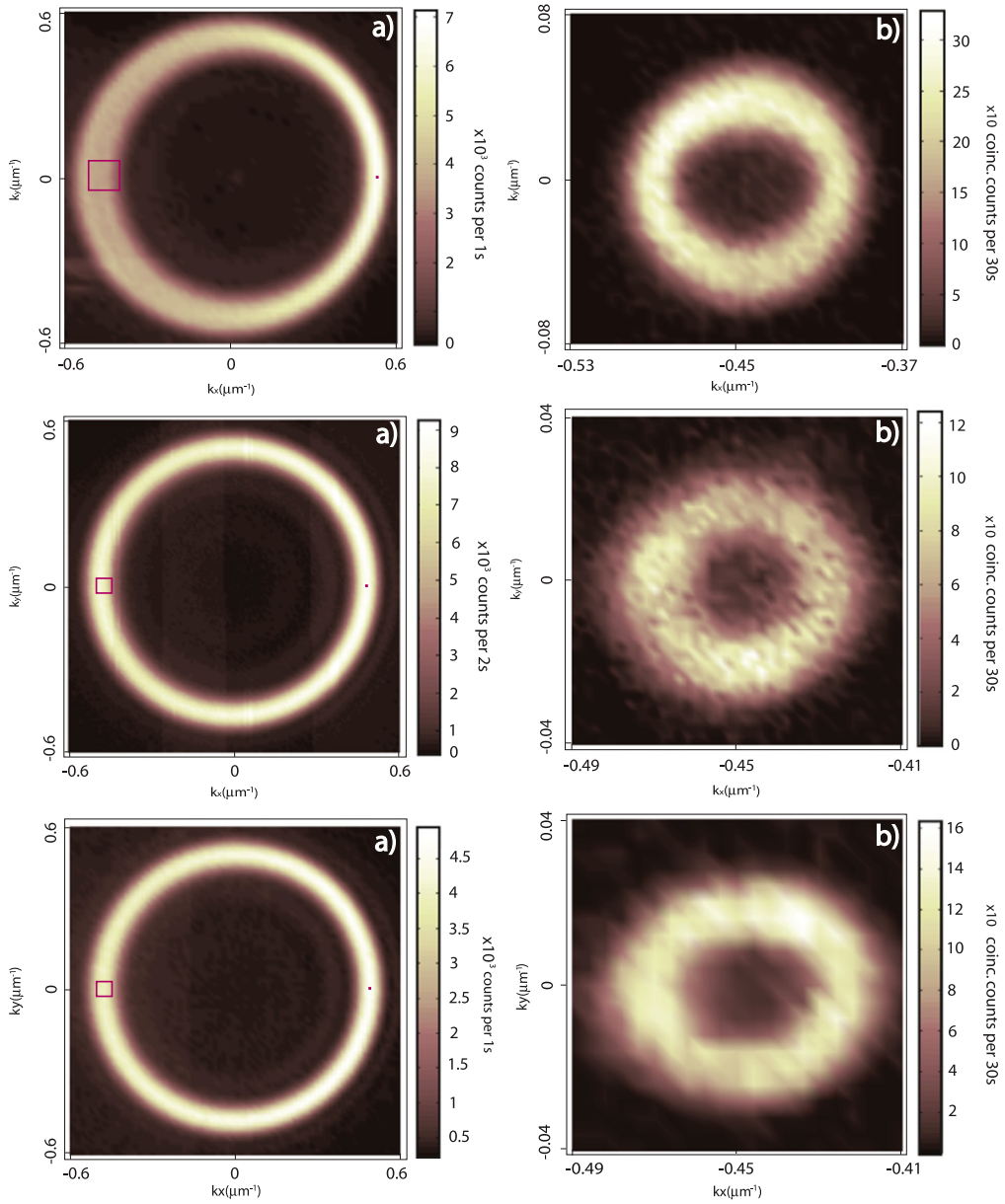

Figure 6. First column: SPDC angular spectrum, second column: conditional angular spectrum. First row: $l = 0$, second row: $l = 1$, and third row: $l = 2$.

show the resulting signal-idler coincidences as a function of the y coordinate, for a number of propagation planes, along z, covering a propagation distance of 40 cm. While figure 8(a) corresponds to $l = 0$, figure 8(b) corresponds to $l = 1$. It can be appreciated that the shape of the signal-mode TI remains essentially unchanged over a propagation distance surpassing 25 cm, with the maximum number of coincidence counts exhibiting a gradual decline, showing a clear indication of inherited non-diffracting behavior at the single photon level.

Besides the observed non-diffractive behavior, we are interested in studying the transfer of OAM from the pump to our heralded single photons, for the case of a BG pump of topological charge $l \geqslant 1$. In order to verify the vortex nature of the heralded signal photons, we placed a diffracting equilateral triangular aperture with sides of 500 μm length on FP2. A lens (focal length $f = 3$ cm) is placed a distance of 3 cm from FP2, so as to define a third Fourier plane (FP3) a distance of 3 cm from the lens. The far field diffraction pattern is obtained by retaining the fixed conditioning idler detector on FP1 and placing a 50 μm diameter fiber tip on FP3; we scan the transverse position of this fiber tip while monitoring signal-idler coincidence counts. The resulting data, i.e coincidence counts between idler photons collected on FP1 and signal photons collected on FP3 as a function of the position of the signal-mode fiber tip constitutes a measurement of the far-field diffracted heralded signal-mode TI. The single-photon diffraction pattern obtained for $l = 1$, shown in figure 9(a), has the expected three-lobe structure, and is very similar to that obtained for the pump (figure 4(e)). Likewise, the diffraction pattern obtained for $l = 2$ (figure 9(b)) has the expected six-lobe structure, and is very similar to that obtained for the pump (figure 4(h)). These results constitute a

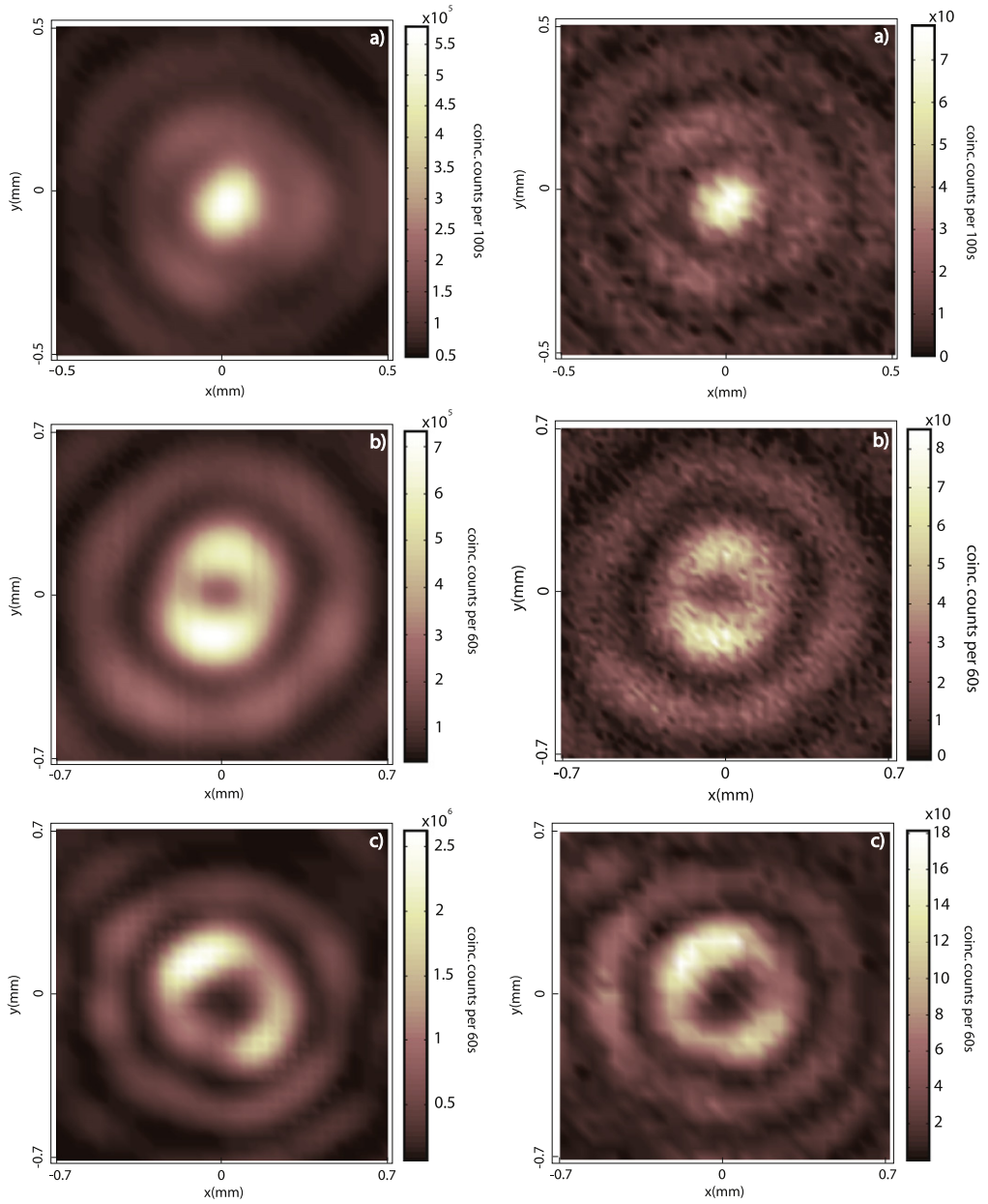

Figure 7. First column: single-photon, signal mode transverse intensity, second column: conditional transverse intensity. First row: $l = 0$, second row: $l = 1$, and third row: $l = 2$.

clear indication that in both cases ($l = 1$ and $l = 2$) the signal-mode heralded single photon is a vortex wave. Thus, we have demonstrated the successful transfer of a classical vortex to the transverse amplitude of the heralded single photon.

4. Conclusions

Our main interest in this work is the preparation of single photons with a configurable transverse shape. For this purpose, we have relied on the SPDC process, together with the use of a structured pump to be used as pump. By resolving the generated photon pairs in transverse wavevector space with standard Fourier optics techniques and detecting an idler photon with a well-defined transverse wavevector, we may herald a single photon in the signal mode with a transverse amplitude which under certain conditions can be identical to the transverse amplitude of the pump. The specific regime in which this transverse amplitude transfer mechanism occurs corresponds to: (i) the use of a sufficiently short crystal, or (ii) the use of a sufficiently compact pump beam in transverse wavevector space, or (iii) an appropriate combination of the latter two conditions.

While transverse amplitude transfer can occur for a pump with an arbitrary transverse structure, in this work we have concentrated on Gaussian and BG beams. For the former, we have both verified that the transverse amplitude transfer

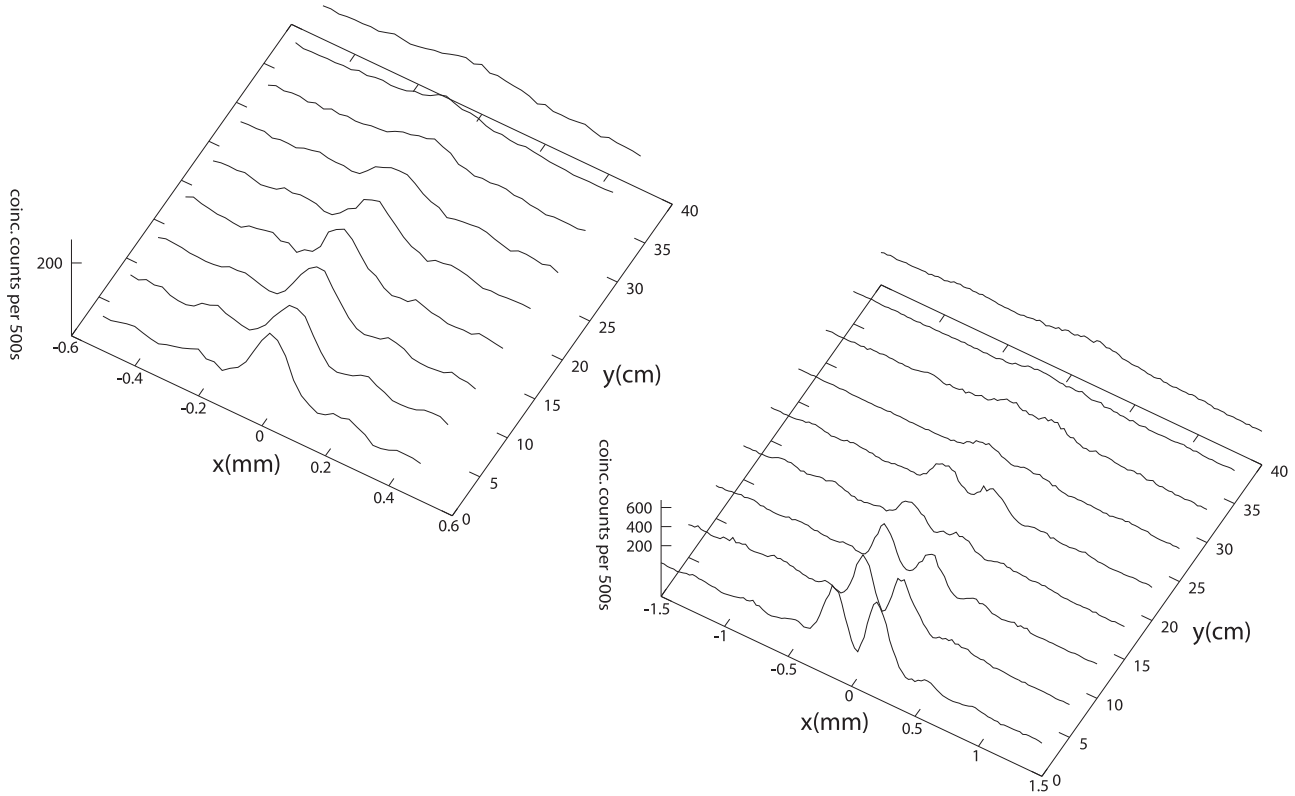

Figure 8. Measured heralded single-photon intensity, as a function of y, under propagation along z, for BG pump of order $l = 0$ (panel a) and $l = 1$ (panel b).

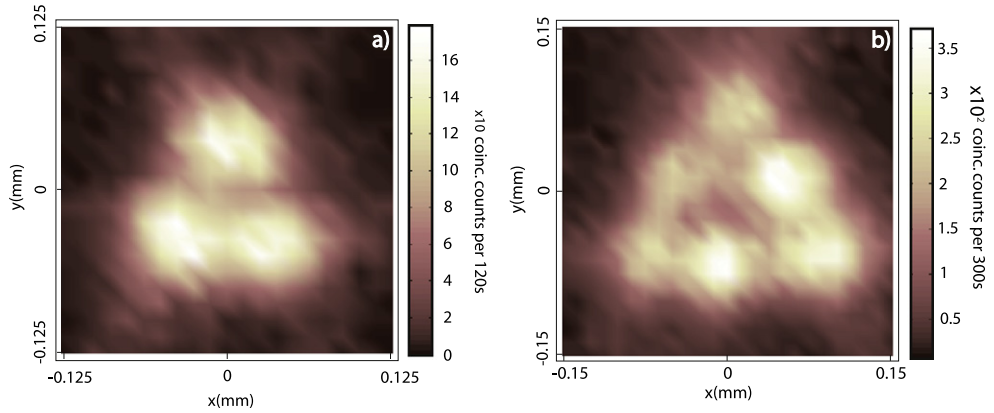

Figure 9. Measured far-field, single-photon diffraction pattern through a triangular aperture, obtained for a BG pump beam of order $l = 1$ (panel a) and $l = 2$ (panel b).

mechanism occurs and studied the effect of a departure from this regime.

BG beams are interesting on a number of fronts. On the one hand, BG beams exhibit a non-diffractive behavior, i.e. the TI remains unchanged over a certain propagation distance. On the other hand, BG beams with orders $l \geqslant 1$ have OAM. In our experiment we implemented high quality BG beams with orders $l = 1$ and $l = 2$ and showed that: (i) within the short-crystal regime the pump AS may be successfully transferred to the signal-mode heralded single photon, (ii) the heralded single photon 'inherits' the non-diffractive behavior from the pump, and (iii) for BG beams of orders $l = 1$ and $l = 2$, the heralded single photon becomes a vortex, with OAM 'inherited' from the pump.

The ability to confer an arbitrary transverse shape to a single photon is an important technology. In our approach, we first shape a (classical) beam as required via phase/amplitude spatial light modulation, and thereafter transfer this shape to a single photon through heralding. We hope that the manipulation of the transverse shape of single photons demonstrated here will be useful for the implementation of quantum information processing schemes which seek to exploit the spatial degree of freedom of single photons.

Acknowledgments

This work was supported in part by grants from SEP-Conacyt (Mexico), PAPIIT (UNAM) IN-111212 and AFOSR grant FA9550-13-1-0071.

References

[1] Monken C H, Souto Ribeiro P H and Pádua S 1998 *Phys. Rev.* A **57** 3123
[2] Walborn S P, Monken C H, Pádua S and Souto Ribeiro P H 2010 *Phys. Rep.* **495** 87
[3] Joobeur A, Saleh B E and Teich M C 1994 *Phys. Rev.* A **50** 3349
[4] Law C K and Eberly J H 2004 *Phys. Rev. Lett.* **92** 127903
[5] Torres J P, Molina-Terriza G and Torner L 2005 *J. Opt. B: Quantum Semiclass. Opt.* **7** 235
[6] Walborn S P, de Oliveira A N, Pádua S and Monken C H 2004 *Phys. Rev. Lett.* **90** 143601
[7] Grayson T P and Barbosa G A 1994 *Phys. Rev.* A **49** 2948
[8] Burnham D C and Weinberg W L 1984 *Phys. Rev. Lett.* **25** 84
[9] Rubin M H 1996 *Phys. Rev.* A **54** 5349–60
[10] Mirhosseini M, Magaña-Loaiza O S, O'Sullivan M N, Rodenburg B, Malik M, Lavery M P J, Padgett M J, Gauthier D J and Boyd R W 2014 arXiv:1402.7113
[11] Barreiro S and Tabosa J W R 2003 *Phys. Rev. Lett.* **90** 133001
[12] Bennink R S, Liu Y, Earl D D and Grice W P 2006 *Phys. Rev.* A **74** 023802
[13] Ramírez-Alarcón R, Cruz-Ramírez H and U'Ren A B 2013 *Laser Phys.* **23** 055204
[14] Walborn S P and Monken C H 2007 *Phys. Rev.* A **76** 062305
[15] Molina-Terriza G, Minardi S, Deyanova Y, Osorio C I, Hendrych M and Torres J P 2005 *Phys. Rev.* A **72** 065802
[16] Saleh B E A, Abouraddy A F, Sergienko A V and Teich M C 2000 *Phys. Rev.* A **62** 043816
[17] di Lorenzo Pires H and van Exter M P 2009 *Phys. Rev.* A **79** 041801
[18] Neves L, Pádua S and Saavedra C 2004 *Phys. Rev.* A **69** 042305
[19] Jha A K and Boyd R W 2010 *Phys. Rev.* A **81** 013828
[20] Lee P S K, van Exter M P and Woerdman W P 2005 *Phys. Rev.* A **72** 033803
[21] Molina-Terriza G, Torres J P and Torner L 2007 *Nat. Phys.* **3** 305
[22] Molina-Terriza G, Torres J P and Torner L 2003 *Opt. Commun.* **228** 155
[23] Arnaut H H and Barbosa G A 2001 *Phys. Rev. Lett.* **85** 286
[24] Walborn S P, de Oliveira A N, Thebaldi R S and Monken C H 2004 *Phys. Rev.* A **69** 023811
[25] Peeters W H, Verstegen E J K and van Exter M P 2007 *Phys. Rev.* A **76** 042302
[26] Ren X F, Guo G P, Li J and Guo G C 2005 *Phys. Lett.* A **341** 81
[27] Kawase D, Miyamoto Y, Takeda M, Sasaki K and Takeuchi S 2009 *J. Opt. Soc. Am.* B **26** 797
[28] Mair A, Vaziri A, Weihs G and Zeilinger A 2001 *Nature* **412** 313
[29] Leach J, Jack B, Romero J, Jha A K, Yao A M, Franke-Arnold S, Ireland D G, Boyd R W, Barnett S M and Padgett M J 2010 *Science* **329** 662
[30] See for example Dada A C, Leach J, Buller G S, Padgett M J and Andersson E 2011 *Nat. Phys.* **7** 677
[31] Durnin J, Micely J J Jr and Eberly J H 1987 *Phys. Rev. Lett.* **58** 1499–501
[32] Turunen J and Friberg A T 2010 *Prog. Opt.* **54** 1–88
[33] Gutierrez-Vega J C and Bandres M A 2005 *J. Opt. Soc. Am.* A **22** 289
[34] Tyler G A and Boyd R W 2009 *Opt. Lett.* **34** 142
[35] Sheng X, Zhu Y, Zhu Y and Zhang Y 2013 *Optik* **124** 2635
[36] McLaren M, Mhlanga T, Padgett M J, Roux F S and Forbes A 2014 *Nat. Commun.* **5** 3248
[37] Cruz-Ramírez H, Ramírez-Alarcón R, Morelos F J, Quinto-Su P, Gutierrez-Vega J C and U'Ren A B 2012 *Opt. Express* **20** 29761
[38] Vicuña-Hernandez V, Cruz-Ramírez H, Ramírez-Alarcón R and U'Ren A B 2014 *Opt. Express* **22** 020027
[39] Klyshko D N 1982 *Zh. Eksp. Teor. Fiz.* **83** 1313
Klyshko D N 1982 *Sov. Phys.—JETP* **56** 753
[40] di Lorenzo Pires H, Coppens F M G J and van Exter M P 2011 *Phys. Rev.* A **83** 033837
[41] Süzer O and Goodson T G III 2008 *Opt. Express* **16** 20166
[42] Grice W P, Bennink R S, Goodman D S and Ryan A T 2011 *Phys. Rev.* A **83** 023810
[43] Vicent L E, U'Ren A B, Rangarajan R, Osorio C I, Torres J P, Zhang L and Walmsley I A 2010 *New J. Phys.* **12** 093027
[44] Fedorov M V, Efremov M A and Volkov P A 2007 *Phys. Rev. Lett.* **99** 063901
[45] Chan K W, Torres J P and Eberly J H 2007 *Phys. Rev.* A **75** 050101
[46] Jeronimo-Moreno Y and U'Ren A B 2009 *Phys. Rev.* A **79** 033839
[47] Tasca D S, Walborn S P, Souto Riberiro P H, Toscano F and Pellat Finet P 2009 *Phys. Rev.* A **79** 033801
[48] Bouchal Z, Wagner J and Chlup M 1998 *Opt. Commun.* **151** 207–11
[49] Gbur G and Korotkova O 2007 *J. Opt. Soc. Am.* A **24** 745–52
[50] Noriega-Manez R J and Gutierrez-Vega J C 2007 *Opt. Express* **15** 16328–41
[51] Hickmann J M, Fonseca E J S, Soares W C and Chavez-Cerda S 2010 *Phys. Rev. Lett.* **105** 053904
[52] Jesus-Silva A J, Fonseca E S and Hickmann J M 2012 *J. Mod. Opt.* **59** 1194
[53] Hickmann J M, Fonseca E J S and Jesus-Silva J 2011 *Europhys. Lett.* **96** 64006